ACS OMEGA

http://pubs.acs.org/journal/acsodf

Article

Biomimetic Polydopamine-Modified Silk Fibroin/Curcumin Nanofibrous Scaffolds for Chemo-photothermal Therapy of Bone Tumor

Zhiyuan Meng, Yichao Liu, Kexiang Xu, Xing Sun, Qingwen Yu, Zhongqing Wu, and Zheng Zhao*

Cite This: *ACS Omega* 2021, 6, 22213−22223

Read Online

ACCESS | Metrics & More | Article Recommendations | Supporting Information

ABSTRACT: The simultaneous therapy of tumor recurrence and bone defects resulting from surgical resection of osteosarcoma is still a challenge in the clinic. Combination therapy based on a localized drug-delivery system shows great promise in the treatment of osteosarcoma. Herein, bifunctional polydopamine (PDA)-modified curcumin (CM)-loaded silk fibroin (SF) composite (SF/CM-PDA) nanofibrous scaffolds, which combined photothermal therapy with chemotherapy to synergistically enhance osteosarcoma therapy, were prepared by PDA coating of the SF/CM nanofibrous scaffolds fabricated by supercritical carbon dioxide (SC-CO_2) technology. The PDA coating improved hydrophilicity and mechanical strength of the SF/CM scaffolds. The SF/CM-PDA scaffolds present good photothermal conversion capacity and excellent photostability. The low pH and near-infrared (NIR) irradiation could effectively accelerate release of CM in the SF/CM-PDA scaffolds. The in vitro anticancer results indicated that the biocompatible SF/CM-PDA scaffolds had a long-term, stable, and superior anticancer effect compared to pure CM. Furthermore, the SF/CM-PDA scaffolds significantly increased the growth inhibition of osteosarcoma MG-63 cells under NIR irradiation (808 nm and 1.3 W/cm^2). Besides, the SF/CM-PDA scaffolds could enhance osteoblast MC3T3-E1 cell proliferation in vitro when the mass ratio of CM was 0.05−0.5%. This work has therefore demonstrated that the bifunctional SF/CM-PDA scaffolds provide a competitive strategy for local osteosarcoma therapy and bone regeneration.

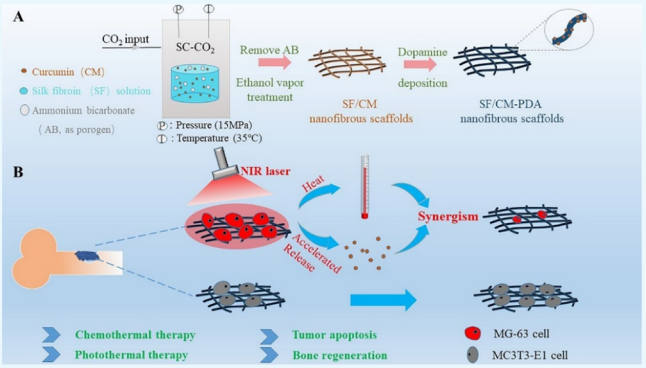

1. INTRODUCTION

Osteosarcoma is the most common primary bone malignant tumor that occurs in children and adolescents.[1,2] In the clinic, the current therapeutic strategy for osteosarcoma is surgical resection.[3] However, tumor recurrence after surgical excision becomes a serious threat to the survival of patients because of incomplete eradication of bone-tumor cells.[4] Moreover, surgery intervention usually leads to great damage to bone tissue,[5] which is hard to be healed by themselves. Therefore, it remains a challenge to develop a bifunctional platform for killing residual tumor cells and repairing bone defects resulting from surgical resection.

Curcumin (CM) is a yellow polyphenol pigment isolated from turmeric and has various biological activities, such as antioxidant, antibacterial, anti-inflammatory, and antitumor activities.[6,7] A study demonstrated that CM could kill osteosarcoma cells induced by hypoxia by downregulating the expression of Notch1.[8] Chen et al. found that CM promoted the cell apoptosis of osteosarcoma cells by downregulating estrogen-related receptor alpha.[9] In recent studies, CM was proved to enhance osteoblastic activity in addition to anticancer activity. Researchers found that when the three-dimensional (3D) printed ceramic scaffold was coated with CM, bone regeneration could be increased by 30 to 45%.[10] Another study also showed that after treatment with 10 μM CM, the proliferation of osteosarcoma cells was decreased by 50%, while the viability of normal osteoblasts was increased by 80%.[11] Unfortunately, the low solubility and bioavailability of CM have limited its application in clinics.

Local drug-delivery systems (LDDSs) have become a potential method to improve the bioavailability of anticancer drugs.[12,13] Nanofibrous scaffold-based LDDSs have a high specific surface area and extracellular matrix (ECM)-like structure, which are beneficial for tissue engineering.[14,15] Silk fibroin (SF), derived from *Bombyx mori*, is usually implied as an implantable fibrous matrix for tumor therapy and bone regeneration.[16,17] Wu et al. adopted the freeze-drying method

Received: June 3, 2021
Accepted: August 13, 2021
Published: August 21, 2021

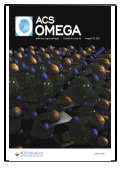

https://doi.org/10.1021/acsomega.1c02903
ACS Omega 2021, 6, 22213−22223

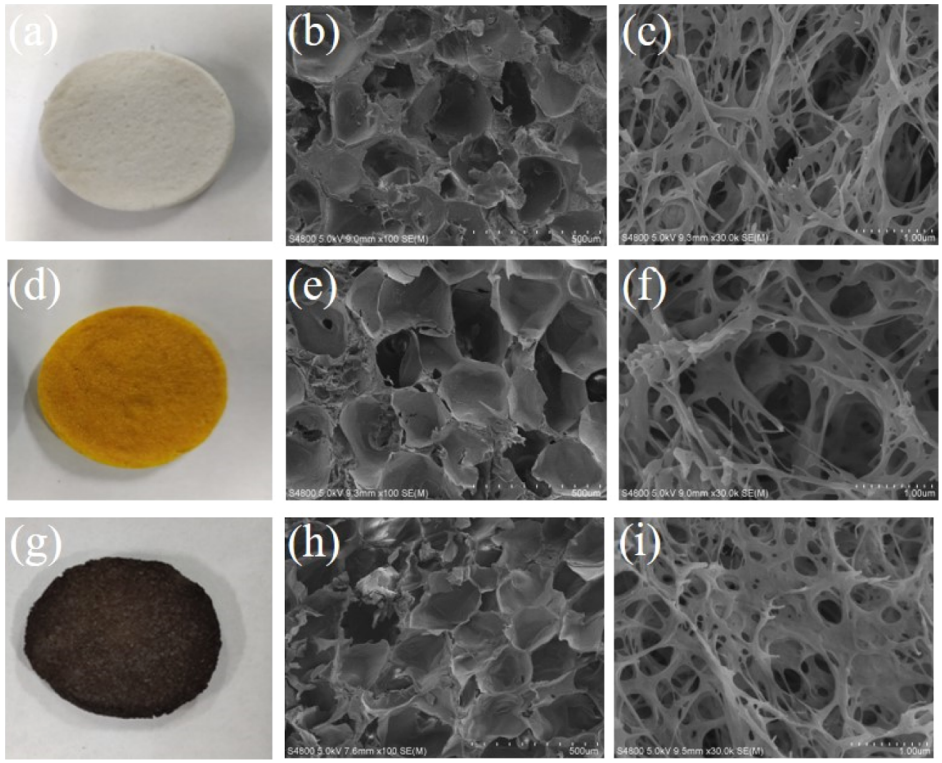

Figure 1. Photograph of SF (a), SF/CM (d), and SF/CM-PDA (g) scaffolds. The corresponding SEM images of the SF (b,c), SF/CM (e,f), and SF/CM-PDA (h,i) scaffolds at different magnifications.

to prepare SF scaffolds with MgO and hydroxyapatite for regeneration of bone tissues.[18] However, nanofibrous structures are difficult to be observed in the lyophilized scaffolds. Electrospinning is a commonly method to prepare nanofibrous matrices in tissue engineering.[19] However, electrospinning leads to limited thickness of 3D porous structures without macropores, which is insufficient for cell seeding and infiltration.[20,21] Supercritical carbon dioxide (SC-CO_2) technology provides an alternative way to fabricate porous scaffolds because of the convenient operation, mild operating conditions, and almost no solvent residue.[14,22] Recently, our group prepared SF scaffolds with nanofibrous structures successfully via SC-CO_2 technology and porogen leaching.[23] The SF-based fibrous scaffolds have been previously reported to be used for delivering various drugs or bioactive molecules.[24,25] However, the study about using SF nanofibrous scaffolds fabricated by SC-CO_2 technology for the delivery of CM to treat osteosarcoma and promote bone regeneration is seldom.

The chemotherapy is difficult to effectively treat tumor because of drug resistance. Recently, photothermal therapy (PTT) has received much attention for tumor treatment owing to its minimal invasiveness, high selectivity, and high treatment efficiency with minimal injury to the surrounding healthy tissues.[26,27] Hyperthermia generated during PTT can directly cause cell apoptosis or necrosis at temperatures above 50 °C. In addition, the accumulation and penetration of chemotherapeutic drugs in tumors can be accelerated by the mild hyperthermia (39−43 °C). Besides, the drug release and uptake can be enhanced.[28,29] Therefore, combining PTT and chemotherapy is an effective approach to enhance the synergistic effect for improved osteosarcoma treatment.

The performance of the photothermal agent determines the effect of photothermal treatment. Polydopamine (PDA), an organic photothermal agent, received substantial interest in tumor therapy and tissue regeneration owing to its strong near-infrared (NIR) light absorption, excellent photothermal conversion efficiency, good biocompatibility, and biodegradability.[30−32] Besides, the structure of PDA is similar to the adhesive proteins of mussels, making it capable to adhere to the surface of various materials as a diverse surface functionalization method.[33,34]

In this study, we report a PDA-functionalized bifunctional fibrous LDDS for localized chemo-photothermal synergistic osteosarcoma therapy and bone regeneration. The SF/CM-PDA nanofibrous scaffolds were prepared by PDA coating of the SF/CM nanofibrous scaffolds fabricated by SC-CO_2 technology. The morphology, chemical structures, water contact angels, mechanical properties, and porosity of the SF/CM-PDA scaffolds were characterized. The drug loading efficiency, pH/NIR responsive behavior, and photothermal properties of the scaffolds were also investigated. The synergic chemotherapy and PTT efficacy of the SF/CM-PDA scaffolds were further studied in vitro. Besides, in vitro osteoblast proliferation analysis was used to investigate the effect of this scaffold on bone tissue regeneration.

2. RESULTS AND DISCUSSION

2.1. Characterization of the SF/CM-PDA Scaffolds. SC-CO_2 technology provides an alternative way to produce 3D scaffolds because of the convenient operation, mild operating conditions, and almost no solvent residue. After extraction of solvents [hexafluoroisopropanol (HFIP) and acetone] by SC-CO_2 and decomposition of ammonium bicarbonate, the SF scaffolds exhibited a white color and interconnected porous

https://doi.org/10.1021/acsomega.1c02903
ACS Omega 2021, 6, 22213−22223

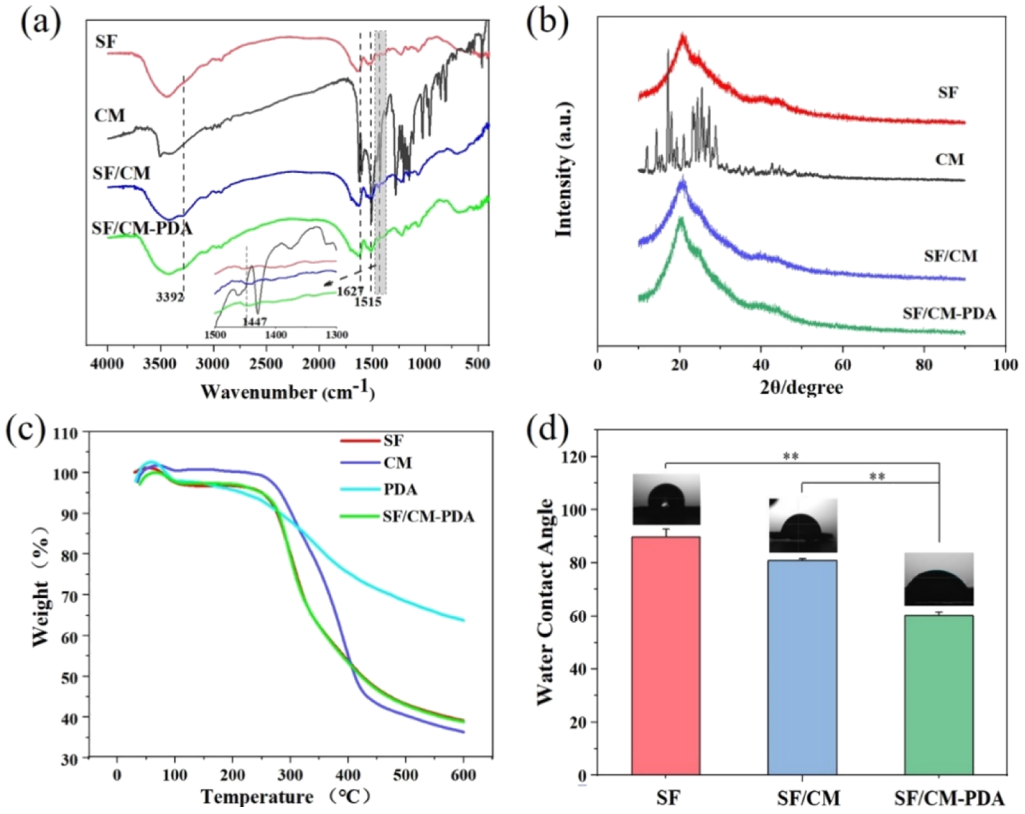

Figure 2. FTIR spectra (a); XRD patterns of original CM, the SF, SF-PDA, SF/CM, and SF/CM-PDA scaffolds (b); thermogravimetric analysis results of pure SF, pure CM, pure PDA, and SF/CM-PDA scaffolds (c); and water contact angle assay (d) (n = 3, *p < 0.05 compared to the SF scaffold group).

and nanofibrous structures (Figure 1a–c), which was beneficial for cell penetration and permeability of nutrients and oxygen. The diameters of the connected nanofibers were below 100 nm, which were in the size range of the collagen fiber in the natural ECM.[35] After CM was encapsulated, the color of the SF/CM scaffolds turned yellow and surface morphology has no obvious change (Figure 1d–f). After PDA coating on the SF/CM scaffolds, the SF/CM-PDA scaffolds exhibited a black color and retained interconnected porous and ECM-like nanofibrous structures (Figure 1g–i).

The results of Fourier transform infrared (FTIR) analysis of original CM, the SF, SF/CM, and SF/CM-PDA scaffolds are shown in Figure 2a. The characteristic peaks at 1640, 1514, and 1239 cm^{-1} correspond to amide groups of SF.[36] The peak at 1450 cm^{-1} attributed to benzene ring vibration of PDA and confirmed the successful deposition of PDA on the SF/CM scaffolds. The characteristic peak at 1628 cm^{-1} corresponding to the stretching vibration of the carbon–carbon double bond of CM indicated the CM incorporation in the SF/CM and SF/CM-PDA scaffolds. These results revealed that the SF/CM-PDA scaffolds were successfully constructed.

Figure 2b shows the X-ray diffraction (XRD) patterns of original CM, the SF scaffolds, SF/CM scaffolds, and SF/CM-PDA scaffolds. A broad diffraction peak at 2θ = 20.7° appeared, implying an amorphous structure of SF in these three kinds of scaffolds.[37] Several high-intensity crystal peaks of original CM were observed in the range of 10–30°, indicating that it was in a highly crystalline form. After the supercritical process, intensity of these characteristic peaks in CM became weak and no visible characteristic peaks of CM could be detected in the SF/CM scaffolds and SF/CM-PDA scaffolds, which indicated that CM in the two scaffolds became a more amorphous state after the supercritical process. The amorphous structure possesses a larger specific volume and higher internal energy, which is helpful to ameliorate the dispersion and bioavailability of CM.[38]

The examination using differential scanning calorimetry measurement (DSC) of pure SF, pure CM, pure PDA, and the SF/CM-PDA scaffolds in a nitrogen atmosphere was conducted (Figure 2c). Nearly 4.5% of the weight loss observed in pure SF at about 35–140 °C was attributed to water evaporation. With the increase in temperature, the weight of the residue began to decrease sharply at 400–500° C due to the thermal degradation of pure SF. After 600 °C, the residual weight was up to 38.16%. The thermal degradation behavior of the SF/CM-PDA scaffolds was similar to that of pure SF. When temperature was increased to 600 °C, the residual weight of the SF/CM-PDA scaffolds, pure CM, and pure PDA was about 39.05, 34.61, and 61.18%, respectively. According to the drug loading analysis, the content of CM in the SF/CM-PDA scaffolds was 1.27%. Based on the above-mentioned results, the content of PDA in the SF/CM-PDA scaffolds could be calculated and was about 4.05%.

The surface hydrophilicity of these scaffolds was also assessed (Figure 2d). The water contact angles of the SF, SF/CM, and SF/CM-PDA scaffolds were 89.78 ± 2.06, 81.02 ± 0.35, and 60.17 ± 0.17°, respectively. Compared to the SF scaffolds and SF/CM scaffolds, an obvious decrease in contact angle value was presented in the SF/CM-PDA scaffolds. These results indicated that PDA coating enhanced the hydrophilicity of the SF/CM scaffolds significantly since PDA contains many hydrophilic functional groups, such as amino and hydroxyl

https://doi.org/10.1021/acsomega.1c02903
ACS Omega 2021, 6, 22213–22223

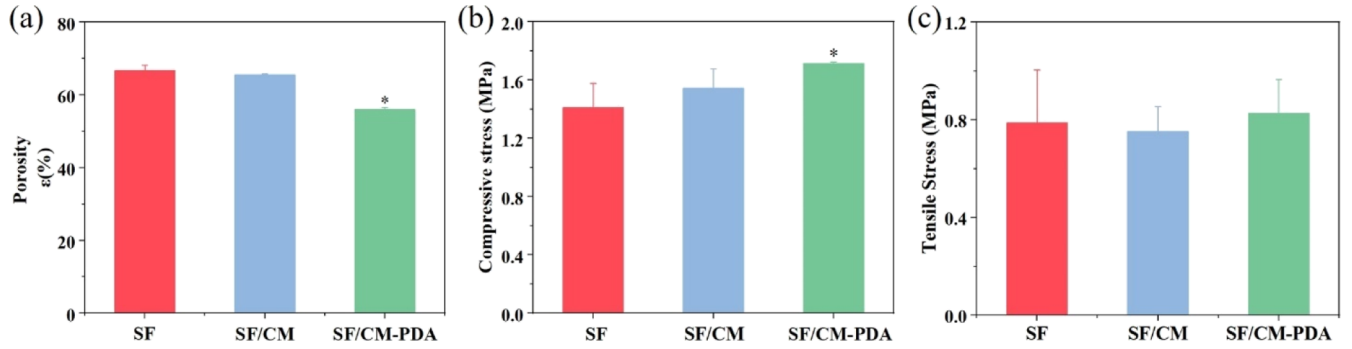

Figure 3. Porosity (a), compressive stress at 25% strain (b), and tensile stress (c) of the SF, SF/CM, and SF/CM-PDA scaffolds.

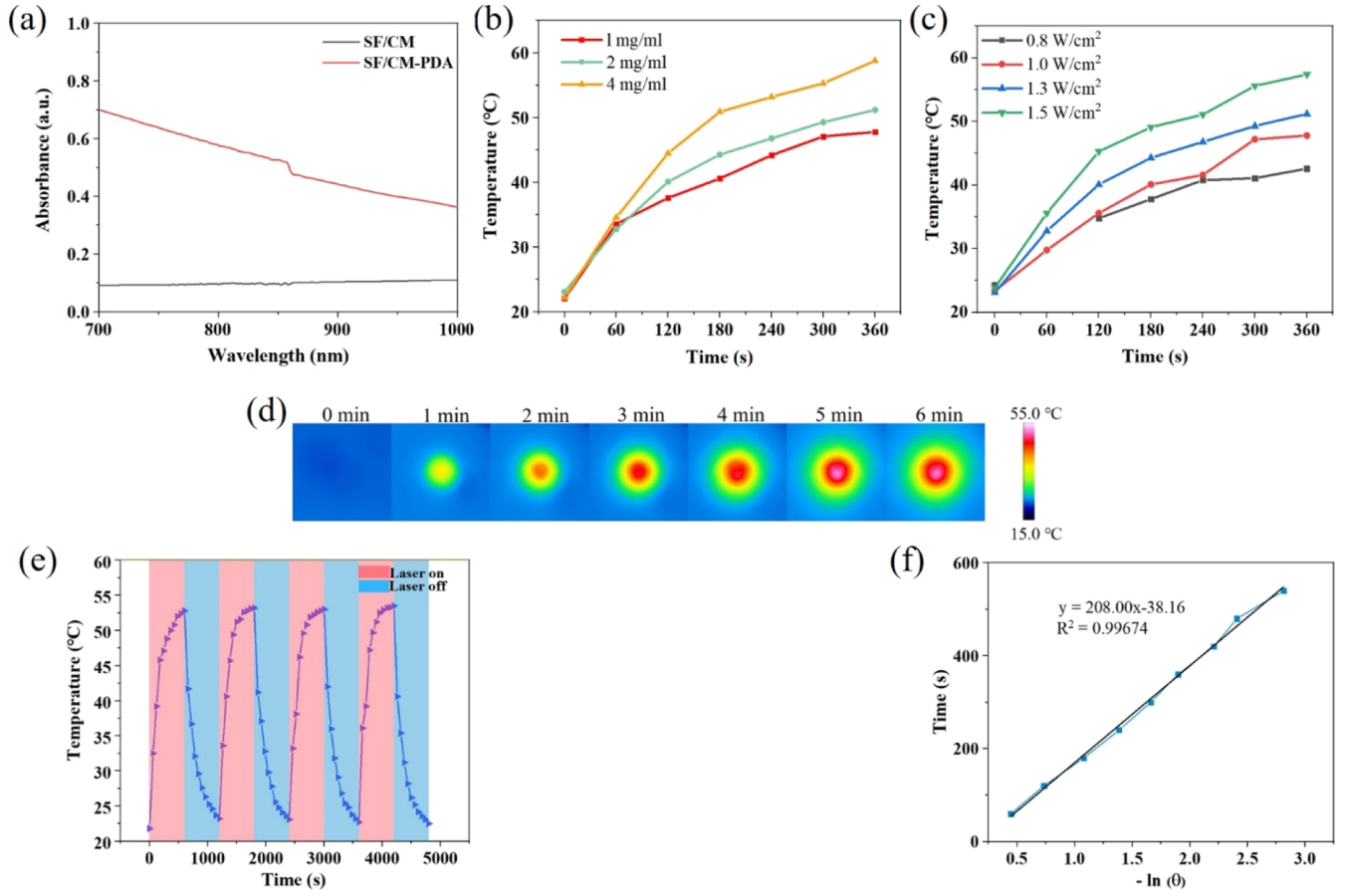

Figure 4. Photothermal property evaluation of SF/CM-PDA scaffolds. UV−vis−NIR spectra of SF/CM and SF/CM-PDA scaffolds (a). Temperature changes in the SF/CM-PDA scaffolds with 808 nm laser irradiation at different laser power densities (0.8, 1.0, 1.3, and 1.5 W/cm^2) (b) and PDA solution (c) for 6 min. Infrared thermal images of the SF/CM-PDA suspension exposed to NIR irradiation (808 nm, 1.3 W/cm^2) for 6 min (d). Temperature change increase in 2 mg/mL PDA solution-functionalized SF/CM-PDA scaffolds over five irradiation cycles (808 nm, 1.3 W/cm^2, and 1200 s intervals) (e). Fitting curves between the time and logarithm of the temperature during the cooling process (f).

groups. The improved hydrophilicity of the SF/CM-PDA scaffolds could be favorable for cell adhesion and proliferation.

2.2. Porosity and Mechanical Property. As shown in Figure 3a, the porosities of the SF, SF/CM, and SF/CM-PDA scaffolds were 66.7, 65.6 and 56.0%, respectively. Obviously, the SF/CM-PDA scaffolds exhibited a lower porosity than the SF and SF/CM scaffolds. After PDA was deposited into the SF/CM scaffolds, PDA coating occupied some space of original pores of the SF/CM scaffolds. Thus, the porosity of the SF/CM-PDA scaffolds decreased.

The compression tests and tensile tests were performed to evaluate the mechanical performance of the scaffolds. As shown in Figure 3b, the compressive strengths of the SF, SF/CM, and SF/CM-PDA scaffolds are 1.41, 1.55, and 1.72 MPa, respectively. Obviously, the SF/CM-PDA scaffolds exhibited higher mechanical properties than the SF scaffolds and SF/CM scaffolds. The formation of interface bonding between the SF/CM matrix and PDA coatings increased the crack propagation resistance of the SF/CM matrix, and the interfacial stress transferred between the PDA and matrix during compression testing.[39] In addition, the homogeneous dispersion of PDA in the SF/CM matrix reduced the stress concentration and minimized the influence of the defects.[40] The increase in compressive strength of the SF/CM-PDA scaffolds with proper

https://doi.org/10.1021/acsomega.1c02903
ACS Omega 2021, 6, 22213−22223

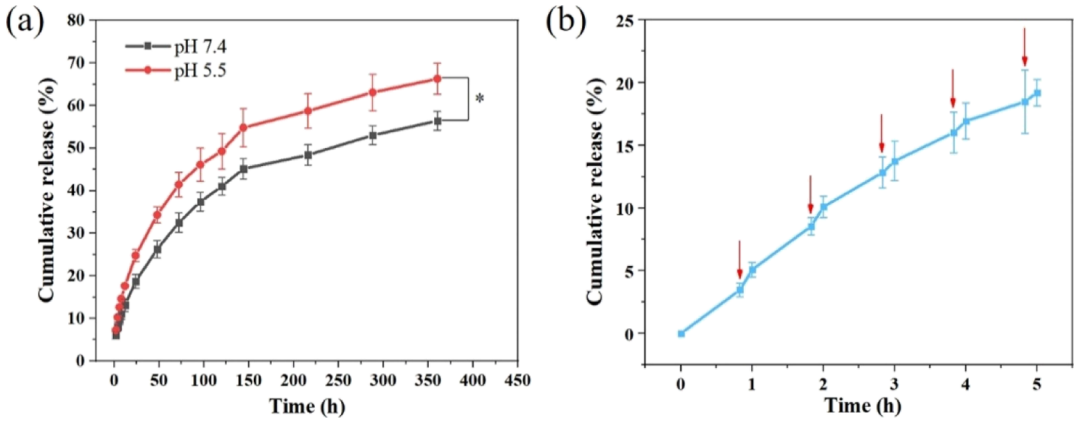

Figure 5. CM release curves from the SF/CM-PDA scaffolds at different pH values (a) and NIR triggered release of CM from the SF/CM-PDA scaffolds (808 nm, 1.3 W/cm^2, and 10 min) (red arrows represent the NIR irradiation) (b).

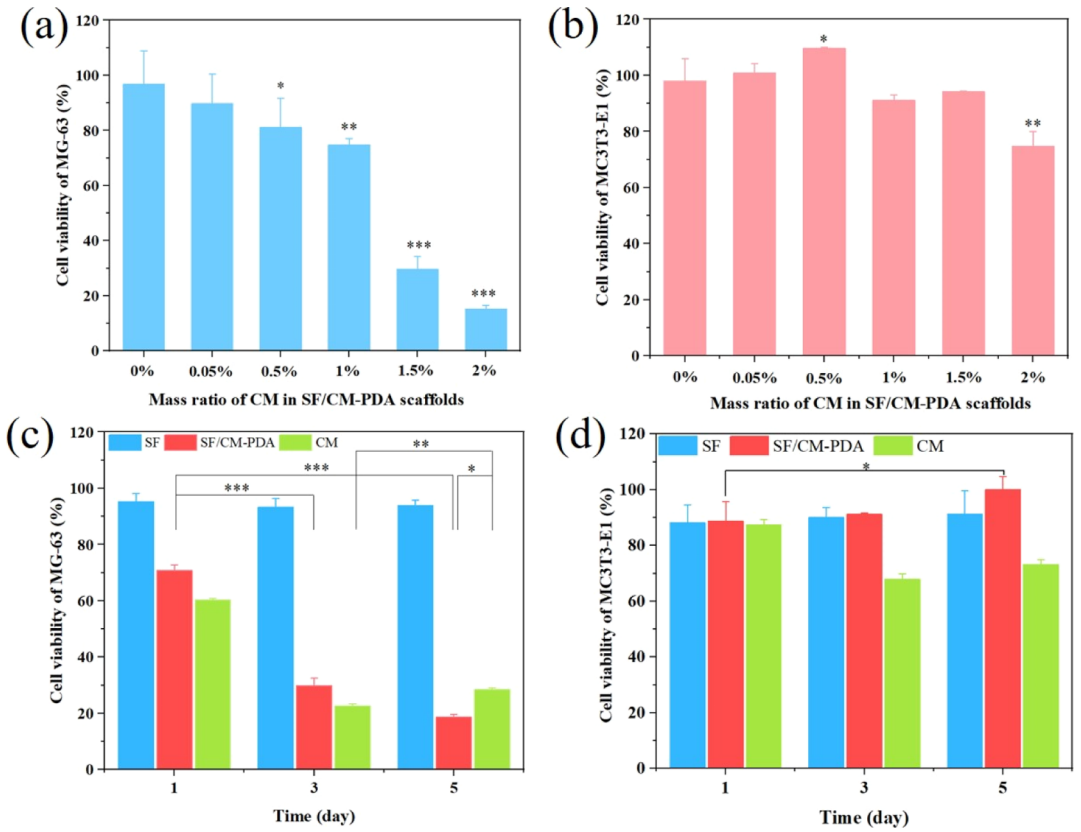

Figure 6. Cell viability of MG-63 cells (a) and MC3T3-E1 cells (b) after incubation with the SF/CM-PDA scaffolds for 72 h. Cell viability of MG-63 cells (c) and MC3T3-E1 cells (d) after being treated with the SF and SF/CM-PDA scaffolds and CM at the same CM concentration level within 5 days. Data are expressed as mean ± standard deviation (n = 6); *p-value < 0.05, **p-value < 0.01, and ***p-value < 0.001.

porosity could better meet the requirements of bone regeneration. As shown in Figure 3c, the tensile strengths were 0.79, 0.75, and 0.83 MPa in the SF, SF/CM, and SF/CM-PDA scaffolds, respectively. Therefore, the addition of CM and PDA coatings did not affect the tensile strength of the SF scaffolds.

2.3. Photothermal Property Evaluation. The results of UV−vis−NIR absorbance spectra demonstrated that the SF/CM-PDA scaffolds exhibited a very strong and broad absorption in the range of 700 and 1000 nm (Figure 4a). Therefore, in order to investigate the photothermal performance of the PDA-functionalized scaffolds, the temperature changes in the SF/CM-PDA scaffolds under NIR irradiation at 808 nm were recorded. With the increase in the concentration of PDA solution, the temperature of scaffolds increased rapidly under NIR irradiation (Figure 4b). The temperature of the 1, 2, and 4 mg/mL PDA solution-functionalized scaffolds could approach to 51.8 and 58.8 °C within 6 min, respectively. These results suggested that the photothermal temperature of the SF/CM-PDA scaffolds improved with the increase in PDA content. As is known, hyperthermia generated during PTT can directly cause cell apoptosis or necrosis at temperatures above 50 °C.[41] Therefore, 2 mg/mL PDA solution had been chosen to functionalize SF/CM scaffolds for treating

https://doi.org/10.1021/acsomega.1c02903
ACS Omega 2021, 6, 22213−22223

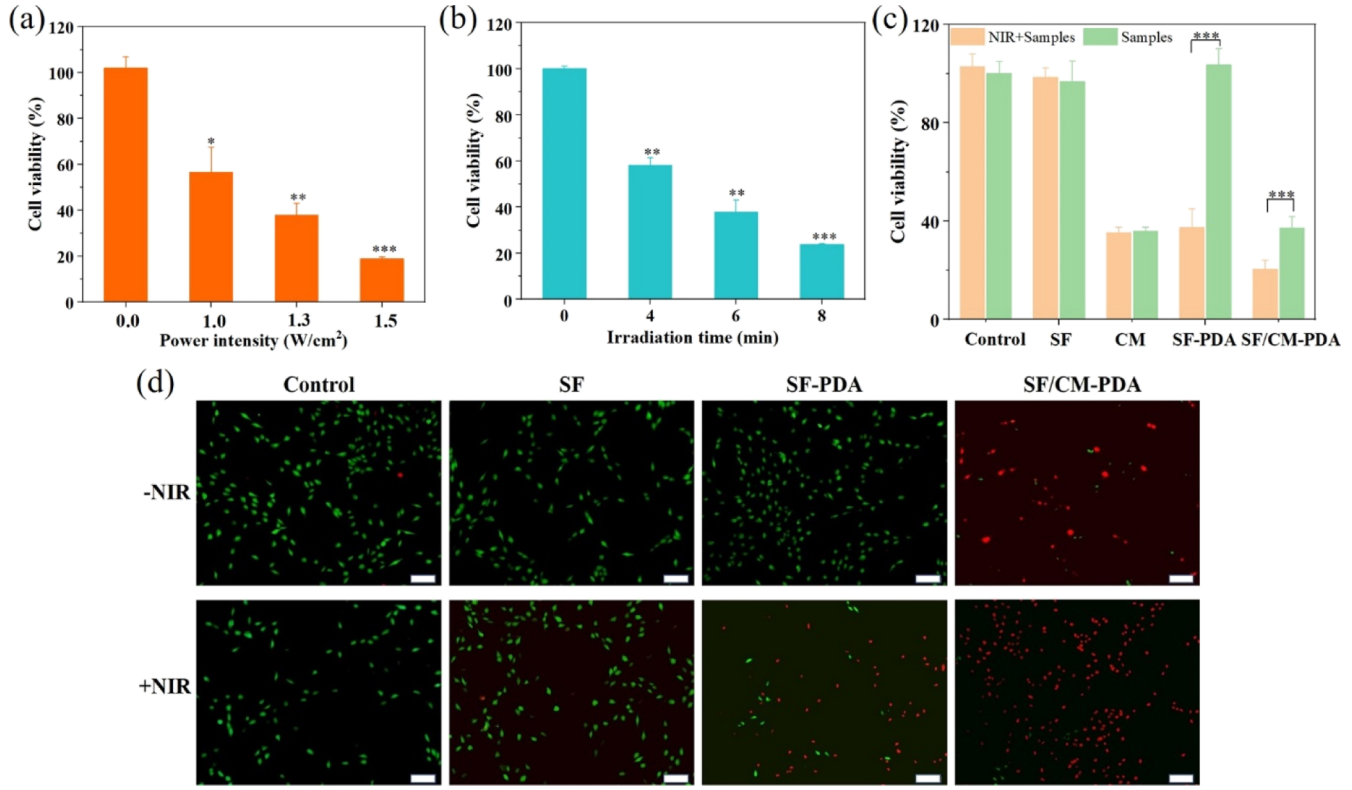

Figure 7. Cell viability of MG-63 cells after being incubated with the SF-PDA scaffolds under different power densities of NIR irradiation (6 min) (a) and under different irradiation times (1.3 W/cm^2) (b). The cell viability of MG-63 cells after being incubated with the SF, SF-PDA, and SF/CM-PDA scaffolds and CM at the same CM concentration level with or without the treatment of the NIR laser (808 nm, 1.3 W/cm^2, and 6 min) (c). Live/dead staining images of MG-63 cells incubated with the SF, SF-PDA, and SF/CM-PDA scaffolds with or without the NIR laser (scale bars: 200 μm) (d).

osteosarcoma. With increasing power densities, the temperature of the SF/CM-PDA scaffolds rapidly went up to over 50 °C after 1.3 and 1.5 W/cm^2 irradiation within 6 min. Figure 4c shows that the photothermal temperature of the SF/CM-PDA scaffolds were time- and laser power density-dependent. The excellent photothermal performance of the SF/CM-PDA scaffolds was due to the intense NIR laser absorption of PDA, and PDA coating could convert the NIR laser into abundant heat energy. Furthermore, the real-time photographs of the scaffolds under irradiation for 6 min obtained by an infrared thermal camera verified the findings mentioned above (Figure 4d). Moreover, the maximum temperature remained at a similar magnitude over four irradiation cycles (Figure 4e), indicating the excellent photostability of the SF/CM-PDA scaffolds. Furthermore, the photothermal conversion efficiency (η) of the SF/CM-PDA scaffolds was calculated to be 23.8% from the cooling curve (Figure 4e) and the corresponding thermal time constant (τ_s) (Figure 4f), which showed that the SF/CM-PDA scaffolds could be utilized as the robust photothermal materials to initiate photothermal conversion for thermal eradication of osteosarcoma under NIR laser irradiation.[42] Therefore, the SF/CM-PDA scaffolds exhibited excellent photothermal performance and could be competent to treat tumor via changing the PDA content and laser power density.

2.4. Anticancer Drug Loading/Responsive Release. To verify the efficient CM loading and controlled release ability of the SF/CM-PDA scaffolds, the CM loading and responsive release in different pH environments and NIR irradiation were conducted. Quantitative analysis showed that the drug loading efficiency of the SF/CM-PDA scaffolds was 85.44%. Cumulative release of CM from the SF/CM-PDA scaffolds, as a function of time, was evaluated in acidic (pH 5.5) and physiological pH (pH 7.4). As viewed from Figure 5a, when the pH value decreased from 7.4 to 5.5, the cumulative release of CM from the scaffolds increased from 55 to 65% after 15 days. The foremost mechanism is accredited to the weakened interaction between SF and CM and faster degradation of SF in the acidic environment.[43] The pH drug-responsive behavior can improve tumor permeation by releasing the drug quickly in the tumor site because solid tumors were in a weakly acidic microenvironment. As seen from the scanning electron microscopy (SEM) images of scaffolds after 15 days of CM release (Figure S1), a more obvious degradation process was observed in pH 5.5 buffer. It is found that the surface became rougher and the diameter of nanofibers was larger because of degradation of the SF matrix and PDA after being immersed in the acid environment. The results were consistent with previous studies.[44,45] It was established that NIR laser irradiation could accelerate the drug release from the NIR-absorbing drug-delivery system because of the rapid increase in local temperature, leading to the weakening of the interactions between the drug and delivery system.[28,46] After NIR irradiation for 10 min at predetermined time intervals, burst release of CM could be observed (Figure 5b), possibly owing to the heat generated by PDA in the SF/CM-PDA scaffolds, which speeded up molecular motion and increased the solubility of CM in the phosphate-buffered saline (PBS) solution. The pH- and NIR-responsive drug release

https://doi.org/10.1021/acsomega.1c02903
ACS Omega 2021, 6, 22213−22223

behavior makes the SF/CM-PDA scaffolds good candidates for the synergic tumor chemo-PTT.

2.5. Interactions of SF/CM-PDA Scaffolds with Osteosarcoma Cells or Osteoblasts In Vitro. In vitro anticancer effect of the SF/CM-PDA scaffolds with different CM contents is shown Figure 6a. Obviously, the SF-PDA scaffolds without CM exhibited no obvious toxicity to MG-63 cells. With the increase in the mass ratio of CM in the SF/CM-PDA scaffolds from 0.05 to 1%, the anticancer effects of scaffolds increased from 89.7 to 74.8%, which implied that CM was a highly dose-sensitive medicine. Moreover, when the mass ratio of CM reached 1.5 and 2%, the cell survival rates decreased to 29.6 and 15.2%, respectively. The results indicated that the SF/CM-PDA scaffolds had good anticancer activity when the mass ratio of CM was over 1%.

Furthermore, the effect of the SF/CM-PDA scaffolds with different CM contents on viability of osteoblasts was investigated (Figure 6b). Obviously, the cell viability of MC3T3-E1 cells was improved, ranging from 100.84 to 109.64%, when the mass ratio of CM increased to 0.05 from 0.5%. With the ratio up to 2%, the viability of MC3T3-E1 cells decreased to 74.71%. The results indicated that SF/CM-PDA scaffolds could enhance osteoblasts proliferation when the mass ratio of CM was 0.05−0.5%. These results demonstrated that the SF/CM-PDA scaffolds enhanced osteoblasts proliferation and had a potential application for treating bone defects after osteosarcoma resection.

When the mass ratio of CM was 1.5%, the SF/CM-PDA scaffolds showed good anticancer activity and exhibited no obvious toxicity toward the osteoblasts. Therefore, the SF/CM-PDA scaffolds with 1.5% CM were chosen to investigate the effects on viability of MG-63 cells in different incubation times. As shown in Figure 6c, the SF scaffolds had no obvious effect on the viability of MG-63 cells after incubation for 1, 3, and 5 days, while CM and SF/CM-PDA scaffolds could significantly decrease the viability of MG-63 cells. With the increase in incubation time, the anticancer activity of the SF/CM-PDA scaffolds was enhanced. However, the anticancer activity of pure CM in 5 days was evidently decreased compared with that in 3 days. It is also noticed that the SF/CM-PDA scaffolds exhibited enhanced better inhibitory activity than pure CM at the same concentration of CM because of the improved bioactivity of CM in the scaffolds, which would decrease the drug resistance and enhance the efficiency of chemotherapy in vivo. Obviously, the SF/CM-PDA scaffolds possessed a long-term, stable, and superior anticancer effect that was probably caused by stable and controlled CM release in the SF/CM-PDA scaffolds to the cells.

The SF/CM-PDA scaffolds with 1.5% CM were also tested to evaluate the long-term in vitro effect on MC3T3-E1 cells. As shown in Figure 6d, with the increase in incubation time, the SF/CM-PDA scaffolds showed increased biocompatibility, while pure CM exhibited mild toxicity. The results might be attributed to the decreased concentration of CM in the SF/CM-PDA scaffolds with increasing time. According to the results of Figure 6b, the SF/CM-PDA scaffolds could enhance osteoblast proliferation when the mass ratio of CM was relatively low. Therefore, with the increase in incubation time, the concentration of CM in the SF/CM-PDA scaffolds decreased, leading to an enhanced effect of osteoblast proliferation. In conclusion, the SF/CM-PDA scaffolds could have a smart treatment potential in bone tumor therapy.

2.6. In Vitro Chemo-PTT Effect. Figure 7a,b shows the effect of the SF-PDA scaffolds under different laser power intensities and irradiation times of the 808 nm laser on cell viability of MG-63 cells. Obviously, with the increase in laser power intensity and irradiation time, the cell viabilities of MG-63 decreased significantly since PDA coating exhibited excellent photothermal performance and could convert the NIR laser into abundant heat energy and cause cell apoptosis directly.

To explore the chemo-photothermal effect of the SF/CM-PDA scaffolds, MG-63 cells were incubated with the scaffolds under NIR irradiation (808 nm, 6 min, and 1.3 W/cm^2). It was shown that the cells did not exhibit obvious growth inhibition when treated with SF + NIR and control + NIR or incubated with the SF-PDA scaffolds and SF scaffolds in the absence of NIR irradiation, indicating the good cytocompatibility of the SF-PDA and SF scaffolds and the safety of laser irradiation (Figure 7c). When MG-63 cells were treated with both the SF-PDA scaffolds and NIR irradiation, the cell viability was decreased to 37.4%. When cells were treated with CM with or without NIR, the cell viability was about 35%. However, when MG-63 cells were treated with the SF/CM-PDA scaffolds under NIR irradiation, cell viability could be decreased to only 20.4%. The in vitro effect of the laser on healthy tissues was also explored. MC3T3-E1 cells were treated with the four samples in the presence of NIR irradiation. The cell viability was decreased in the SF-PDA + NIR group. However, no statistical difference ($p > 0.05$) was found between the SF/CM-PDA group and SF/CM-PDA + NIR group (Figure S2). It could be concluded that the tumor cells were more sensitive to laser-induced hyperthermia compared to normal cells. The fluorescence images of live and dead assay also showed that the SF/CM-PDA scaffolds killed more osteosarcoma cells than the SF-PDA scaffolds under NIR irradiation (Figure 7d), which resulted from the heat-induced and accelerated CM release in the presence of NIR irradiation. These results confirmed that the SF/CM-PDA scaffolds enabled the chemo-photothermal synergetic antitumor efficiency in vitro. The evident in vitro synergic therapy effect of the SF/CM-PDA scaffolds would guide us to explore the in vivo bone tumor inhibition effect of the SF/CM-PDA scaffolds in further study.

3. CONCLUSIONS

In summary, we developed implantable therapeutic platform SF/CM-PDA scaffolds with interconnected porous and ECM-like nanofibrous structures for chemo-photothermal tumor therapy. The deposition of PDA on the surface of scaffolds improved hydrophilicity and mechanical strength of the SF/CM scaffolds. Meanwhile, the SF/CM-PDA scaffolds showed excellent photothermal properties and a typical pH- and NIR-controlled CM release behavior. Moreover, the SF/CM-PDA scaffolds exhibited dose- and time-dependent inhibition effect on the growth of MG-63 cells. More importantly, the growth and activity of MG-63 cells were effectively inhibited by the synergetic chemo-PTT effect in vitro. Additionally, the SF/CM-PDA scaffolds could promote the proliferation of MC3T3-E1 cells in vitro when the mass ratio of CM was 0.05−0.5%. As biocompatible biomaterials, the SF/CM-PDA bifunctional scaffolds have great potential for the treatment of osteosarcoma and tumor-related bone defect repair.

https://doi.org/10.1021/acsomega.1c02903
ACS Omega 2021, 6, 22213−22223

4. MATERIALS AND METHODS

4.1. Materials. *B. mori* raw silk was purchased from Suzhou Soho Biomaterials Science & Technology Co. Ltd (China). CO_2 was supplied by WuHanShi XiangYun Industry Co. Ltd (China). HFIP was from Aladdin (USA). CM and dopamine hydrochloride were supplied by Aladdin Industrial Co. Ltd (China). Tris−HCl solution (1 M, pH 8.5) was purchased from Beyotime Biotechnology Co (China). The MC3T3-E1 and MG-63 cells were obtained from China Center for Type Culture Collection (China).

4.2. Preparation of Pure SF. *B. mori* cocoons were degummed by boiling for 2 h in a 0.02 M aqueous Na_2CO_3 solution to remove the sericines and then washed with distilled water three times. Subsequently, degummed SF fibers were dissolved in a solution of $CaCl_2/H_2O$/ethanol in a molar ratio of 1:8:2 for 3 h at 80 °C. Then, this solution was dialyzed in distilled water for 4 days to obtain pure SF solution. Subsequently, the resultant solution was frozen at −20 °C for 12 h, and the pure SF was obtained by lyophilization for 72 h with a freeze dryer.

4.3. Fabrication of the SF/CM-PDA Nanofibrous Scaffolds. SC-CO_2 technology was employed to fabricate the SF, SF-PDA, and SF/CM-PDA nanofibrous scaffolds. Briefly, the SF solution was first prepared at a concentration of 10% (w/v) by dissolving the lyophilized SF material in HFIP to obtain a homogeneous solution. Then, 5 mL of SF solution was cross-linked with 1.2 mL of acetone to form a gel. Subsequently, the mixture was spread in a glass bar, the thickness of the gel being 1−2 mm. It was then transferred to the supercritical fluid device (SFE-2, Nantong Yichuang Co. Ltd., China) and pressurized with CO_2 at 35 °C and 15 MPa for 4−8 h. In order to prepare the SF/CM nanofibrous scaffolds, 1.5% (w/w) CM was dissolved in the SF solution. After the SC-CO_2 process, the obtained scaffolds were treated within atmospheres of 75% ethanol vapor to induce crystallization and insolubility in water for 6 h and then dried in an oven at 40 °C for 24 h to remove ammonium bicarbonate. The SF-PDA and SF/CM-PDA nanofibrous scaffolds were achieved by depositing dopamine on the SF and SF/CM nanofibrous scaffolds, respectively. After being immersed in the Tris buffer solution (2 mg/mL, pH 8.5) of dopamine hydrochloride solution for 24 h at room temperature, the SF-PDA and SF/CM-PDA nanofibrous scaffolds were retrieved and washed three times with Tris−HCl solution and deionized water and finally lyophilized under vacuum.

4.4. Characterization of SF/CM-PDA Scaffolds. Morphological analysis of nanofibrous scaffolds was carried out through SEM (S-4800, Hitach, Japan). The chemical structure of scaffolds was analyzed by infrared spectroscopy (FTIR; Nicolet 6700, Thermo Electron Scientific Instrument, USA) within the wavenumber range of 4000−400 cm^{-1}. The crystallinity of samples was evaluated using an X-ray diffractometer (D8 Advance, Bruker AXS, Germany) with Cu Kα (λ = 1.5405 Å) radiation. The measurement was performed in a diffraction angle ranging from 5 to 45° at a speed of 6°/min with a two-dimensional detector at 40 kV and 40 mA. The characteristics of pure SF, CM, pure PDA, and SF/CM-PDA scaffolds were detected with the DSC instrument (DSC8500, USA). The experiment was performed in a nitrogen environment in a dynamic mode with a heating rate of 10 °C/min; the temperature range was from 30 to 600 °C. The surface hydrophilicity of various nanofibrous matrices was evaluated by measuring the water contact angle (Theta Lite 3100, Biolin Scientific, Finland). The UV−vis−NIR absorbance of the SF/CM-PDA scaffolds was recorded on a UV−vis−NIR spectrophotometer (Lambda 750 S, PerkinElmer).

4.5. Mechanical Performance and Porosity. The compressive strength of the SF, SF/CM, and SF/CM-PDA scaffolds were measured to assess the mechanical strength of each scaffolds using a universal testing system (Instron 5967, China) at room temperature. Cylindrical samples were 10 mm in diameter and 15 mm in height. A 0.1 kN load cell and a 1 mm/min crosshead speed were selected. Then, the 25% compressive strain of the scaffolds was determined to be the compressive strength according to ISO 604:2002.

To determine tensile strength, all the samples were made into a specific shape (15 mm in length, 8 mm in width, and a thickness that was measured before examination). Then, samples were stretched at a clamp speed of 2 mm/min. The average tensile breaking strength was determined to be the tensile strength.

The porosity of the SF, SF/CM, and SF/CM-PDA scaffolds were measured by the pycnometer method. Under constant temperature conditions, the total weight of the pycnometer filled with ethanol was measured as W_1, and the sample with a known mass of W_S was immersed into ethanol. After ethanol filled the pores of the sample, extra ethanol was added until samples became saturated, and the total weight of the pycnometer was recorded as W_2. The sample soaked with ethanol was taken out. Subsequently, the remaining weight of ethanol and pycnometer was recorded as W_3 after samples were removed. Finally, the porosity ε (%) was determined using the following formula

$$\varepsilon\ (\%) = \frac{V_p}{V_p + V_s} \times 100\% = \frac{W_2 - W_3 - W_s}{W_1 - W_3} \times 100\%$$

The volume of samples is V_s and the volume of the inner pores of the sample is V_p.

All samples were measured three times for each group.

4.6. Photothermal Performance of Scaffolds. The photothermal performance of the scaffolds was investigated by monitoring the temperature changes in the SF/CM-PDA scaffolds under NIR laser irradiation. Briefly, the scaffolds were placed in a 48-well plate and then irradiated with an 808 nm laser (MDL-H-808-5W-BJ00440) for 6 min in 500 μL of PBS. The temperature changes in the scaffolds with different PDA concentrations (1, 2, and 4 mg/mL) and different laser power densities (0.8, 1.0, 1.3, and 1.5 W/cm^2) were recorded using a visual thermometer every 1 min. Meanwhile, the photothermal stability of the scaffolds was explored for four cycles of irradiation. The scaffolds were irradiated for 5 min by the 808 nm NIR laser to reach the highest temperature (laser on); then, the laser was turned off and the scaffolds were naturally cooled to room temperature (laser off). Four laser on/laser off cycles were conducted. The photothermal conversion efficiency (η) was calculated according to the reported method[47]

$$\eta = \frac{hS(T_{max} - T_{surr}) - hS(T_{max,water} - T_{surr})}{I(1 - 10^{-A_{808}})}$$

h is the heat transfer coefficient, S is the surface area of the container, I is the laser power, and A is the absorbance of the photothermal material at 808 nm.

https://doi.org/10.1021/acsomega.1c02903
ACS Omega 2021, 6, 22213−22223

$$\tau_s = \frac{mc}{hS}$$

m is the mass of the solution containing the photothermal materials, C is the heat capacity of the solution (C_{water} = 4.2 J/(g·°C)), and τ_s is the associated time constant.

$$t = -\tau_s \ln \theta$$

θ which is defined as

$$\theta = \frac{T - T_{surr}}{T_{max} - T_{surr}}$$

4.7. In Vitro Drug pH/NIR-Controlled Release Behavior Study. The drug release kinetics was investigated by incubating 15 mg of the SF/CM-PDA scaffolds in 5 mL of PBS containing 1% v/v of Tween 80 (to maintain a sink condition) with different pH values (pH = 7.4 and 5.5) under gently stirring at 37 °C. In addition, the scaffolds were also exposed to 808 nm NIR irradiation (1.3 W/cm^2) for 10 min in PBS (pH = 7.4) to demonstrate the property of NIR-triggered drug release. At each time interval, 5 mL of buffer solution was collected. At the same time, the same volume of fresh PBS was added. The UV−vis spectra and corresponding standard calibration curve were used to determine the released drug amount. All samples were prepared in triplicate.

4.8. Cell Culture and Proliferation. Human osteosarcoma cells (MG-63) and mouse preosteoblast cells (MC3T3-E1) were cultured in minimum Eagle's essential medium (MEM) and α-MEM, respectively, both supplemented with 10% fetal bovine serum (FBS) and 1% penicillin/streptomycin. Cells were incubated in a humidified incubator containing 5% CO_2 at 37, and the cell culture medium was replaced every 3 days.

4.9. Interactions of SF/CM-PDA Scaffolds with Osteosarcoma Cells or Osteoblasts In Vitro. MC3T3-E1 and MG-63 cells were seeded on the different CM mass ratios of the SF/CM-PDA scaffolds in the 48-well plates (5000 cells/well). After 72 h of coculture, the cell viability was evaluated by MTS dye (Promega). Briefly, the culture medium was aspirated, and cells were washed with PBS three times. Then, 100 μL of the MTS solution mixed with 500 μL of fresh serum free medium was added for another 4 h of incubation. The absorbance values were measured using a microplate reader (Thermo Scientific, USA) at 490 nm. Cell viability was calculated using the equation below

$$\text{cell viability (\%)} = \frac{\text{absorbance of test cells}}{\text{absorbance of control}} \times 100$$

where absorbance of test cells represents the OD_{490} values of cells treated with different experimental groups and the absorbance of control cells refers to the OD_{490} values of nontreated cells in the control groups.

4.10. In Vitro Chemo-PTT Evaluation. In order to determine proper PTT conditions, we first studied the cell viability of MG-63 cells cultured with the SF-PDA scaffolds under different laser power densities and irradiation times. The in vitro thermo-chemotherapy efficiency was subsequently investigated by evaluating the cell survival rate after being treated with the SF/CM-PDA, SF-PDA, and SF scaffolds and CM under laser irradiation. Typically, MG-63 cells were seeded on various nanofibrous matrices and cultured in 48-well at a density of 5000 cells/well under standard conditions for 48 h. Subsequently, the cells treated with various nanofibrous matrices were exposed to the NIR laser for 6 min. After laser irradiation, the cells were further cultured for 12 h. Finally, the cell viability was evaluated by MTS assay. The same procedures were performed for MC3T3-E1 cells to explore the in vitro effect of the laser on healthy tissues.

In order to investigate the photothermal effect on MG-63 cells more directly, a live/dead assay was carried out. The cells were treated with or without laser irradiation; then, the samples were washed with PBS three times, and MG-63 cells were stained with the calcein-AM/PI stain reagent for 30 min, and the state of the cells was observed using a fluorescent microscope (OLYMPUS, Japan).

4.11. Statistical Analysis. The data were statistically analyzed by SPSS19.0. Using the one-way ANOVA test, statistical significances between groups were marked with (*) for p value < 0.05, (**) for p-value < 0.01, and (***) for p-value < 0.001.

■ ASSOCIATED CONTENT

Supporting Information

The Supporting Information is available free of charge at https://pubs.acs.org/doi/10.1021/acsomega.1c02903.

SEM images of SF/CM-PDA scaffolds after 15 days of drug release in different pH values and assay of in vitro chemo-photothermal therapy on the MC3T3-E1 cells (PDF)

■ AUTHOR INFORMATION

Corresponding Author

Zheng Zhao − *State Key Laboratory of Advanced Technology for Materials Synthesis and Processing, Wuhan University of Technology, Wuhan 430070, China*; Email: zhengzhao@whut.edu.cn

Authors

Zhiyuan Meng − *State Key Laboratory of Advanced Technology for Materials Synthesis and Processing, Wuhan University of Technology, Wuhan 430070, China*; orcid.org/0000-0002-4316-7201

Yichao Liu − *Center for Evidence-Based and Translational Medicine, Zhongnan Hospital of Wuhan University, Wuhan 430071, China*

Kexiang Xu − *State Key Laboratory of Advanced Technology for Materials Synthesis and Processing, Wuhan University of Technology, Wuhan 430070, China*

Xing Sun − *State Key Laboratory of Advanced Technology for Materials Synthesis and Processing, Wuhan University of Technology, Wuhan 430070, China*; orcid.org/0000-0003-2456-9616

Qingwen Yu − *State Key Laboratory of Advanced Technology for Materials Synthesis and Processing, Wuhan University of Technology, Wuhan 430070, China*

Zhongqing Wu − *State Key Laboratory of Advanced Technology for Materials Synthesis and Processing, Wuhan University of Technology, Wuhan 430070, China*

Complete contact information is available at: https://pubs.acs.org/10.1021/acsomega.1c02903

Notes

The authors declare no competing financial interest.

■ ACKNOWLEDGMENTS

This work was supported by the National Natural Science Foundation of China (52073220, 51803160, and 11905161), the National Key Research and Development Program of China (2018YFB1105500), and the Young TopNotch Talents Fund of Wuhan University of Technology (471-40120093).

■ REFERENCES

(1) Longhi, A.; Errani, C.; De Paolis, M.; Mercuri, M.; Bacci, G. Primary bone osteosarcoma in the pediatric age: state of the art. *Cancer Treat. Rev.* **2006**, *32*, 423−436.
(2) Tiram, G.; Segal, E.; Krivitsky, A.; Shreberk-Hassidim, R.; Ferber, S.; Ofek, P.; Udagawa, T.; Edry, L.; Shomron, N.; Roniger, M.; Kerem, B.; Shaked, Y.; Aviel-Ronen, S.; Barshack, I.; Calderón, M.; Haag, R.; Satchi-Fainaro, R. Identification of Dormancy-Associated MicroRNAs for the Design of Osteosarcoma-Targeted Dendritic Polyglycerol Nanopolyplexes. *ACS Nano* **2016**, *10*, 2028−2045.
(3) Luetke, A.; Meyers, P. A.; Lewis, I.; Juergens, H. Osteosarcoma treatment - where do we stand? A state of the art review. *Cancer Treat. Rev.* **2014**, *40*, 523−532.
(4) Isakoff, M. S.; Bielack, S. S.; Meltzer, P.; Gorlick, R. Osteosarcoma: Current Treatment and a Collaborative Pathway to Success. *J. Clin. Oncol.* **2015**, *33*, 3029−3035.
(5) Reichert, J. C.; Saifzadeh, S.; Wullschleger, M. E.; Epari, D. R.; Schütz, M. A.; Duda, G. N.; Schell, H.; van Griensven, M.; Redl, H.; Hutmacher, D. W. The challenge of establishing preclinical models for segmental bone defect research. *Biomaterials* **2009**, *30*, 2149−2163.
(6) Dai, Y.; Jiang, Z.; Li, J.; Wang, M.; Liu, C.; Qi, W.; Su, R.; He, Z. Co-assembly of curcumin and a cystine bridged peptide to construct tumor-responsive nano-micelles for efficient chemotherapy. *J. Mater. Chem. B* **2020**, *8*, 1944−1951.
(7) Saghatelyan, T.; Tananyan, A.; Janoyan, N.; Tadevosyan, A.; Petrosyan, H.; Hovhannisyan, A.; Hayrapetyan, L.; Arustamyan, M.; Arnhold, J.; Rotmann, A.-R.; Hovhannisyan, A.; Panossian, A. Efficacy and safety of curcumin in combination with paclitaxel in patients with advanced, metastatic breast cancer: A comparative, randomized, double-blind, placebo-controlled clinical trial. *Phytomedicine* **2020**, *70*, 153218.
(8) Wang, Z.; Zhang, K.; Zhu, Y.; Wang, D.; Shao, Y.; Zhang, J. Curcumin inhibits hypoxia-induced proliferation and invasion of MG-63 osteosarcoma cells via downregulating Notch1. *Mol. Med. Rep.* **2017**, *15*, 1747−1752.
(9) Chen, P.; Wang, H.; Yang, F.; Chen, H.; He, W.; Wang, J. Curcumin Promotes Osteosarcoma Cell Death by Activating miR-125a/ERRα Signal Pathway. *J. Cell. Biochem.* **2017**, *118*, 74−81.
(10) Bose, S.; Sarkar, N.; Banerjee, D. Effects of PCL, PEG and PLGA polymers on curcumin release from calcium phosphate matrix for in vitro and in vivo bone regeneration. *Mater. Today Chem.* **2018**, *8*, 110−120.
(11) Webster, T. J.; Sun, L.; Chang, K. Short communication: selective cytotoxicity of curcumin on osteosarcoma cells compared to healthy osteoblasts. *Int. J. Nanomed.* **2014**, *9*, 461−465.
(12) Tabet, A.; Jensen, M. P.; Parkins, C. C.; Patil, P. G.; Watts, C.; Scherman, O. A. Designing Next-Generation Local Drug Delivery Vehicles for Glioblastoma Adjuvant Chemotherapy: Lessons from the Clinic. *Adv. Healthcare Mater.* **2019**, *8*, 1801391.
(13) Wolinsky, J. B.; Colson, Y. L.; Grinstaff, M. W. Local drug delivery strategies for cancer treatment: gels, nanoparticles, polymeric films, rods, and wafers. *J. Controlled Release* **2012**, *159*, 14−26.
(14) Deng, A.; Chen, A.; Wang, S.; Li, Y.; Liu, Y.; Cheng, X.; Zhao, Z.; Lin, D. Porous nanostructured poly-l-lactide scaffolds prepared by phase inversion using supercritical CO2 as a nonsolvent in the presence of ammonium bicarbonate particles. *J. Supercrit. Fluids* **2013**, *77*, 110−116.
(15) Wang, Y.; Cao, Z.; Cheng, R.; Qin, M.; Zhang, D.; Deng, L.; Chen, X.; Cui, W. Immunomodulated electrospun fibrous scaffolds via bFGF camouflage for pelvic regeneration. *Appl. Mater. Today* **2019**, *15*, 570−581.
(16) Asadpour, S.; Kargozar, S.; Moradi, L.; Ai, A.; Nosrati, H.; Ai, J. Natural biomacromolecule based composite scaffolds from silk fibroin, gelatin and chitosan toward tissue engineering applications. *Int. J. Biol. Macromol.* **2020**, *154*, 1285−1294.
(17) Xie, X.; Liu, L.; Zheng, Z.; Han, Z.; Zhi, M.; Kaplan, D. L.; Li, G.; Wang, X. Silk Fibroin-Based Fibrous Anal Fistula Plug with Drug Delivery Function. *Macromol. Biosci.* **2018**, *18*, 1700384.
(18) Wu, Z.; Meng, Z.; Wu, Q.; Zeng, D.; Guo, Z.; Yao, J.; Bian, Y.; Gu, Y.; Cheng, S.; Peng, L.; Zhao, Y. Biomimetic and osteogenic 3D silk fibroin composite scaffolds with nano MgO and mineralized hydroxyapatite for bone regeneration. *J. Tissue Eng.* **2020**, *11*, 204173142096779.
(19) Min, B.-M.; Lee, G.; Kim, S. H.; Nam, Y. S.; Lee, T. S.; Park, W. H. Electrospinning of silk fibroin nanofibers and its effect on the adhesion and spreading of normal human keratinocytes and fibroblasts in vitro. *Biomaterials* **2004**, *25*, 1289−1297.
(20) Bongiovanni Abel, S.; Montini Ballarin, F.; Abraham, G. A. Combination of electrospinning with other techniques for the fabrication of 3D polymeric and composite nanofibrous scaffolds with improved cellular interactions. *Nanotechnology* **2020**, *31*, 172002.
(21) Jayarama Reddy, V.; Radhakrishnan, S.; Ravichandran, R.; Mukherjee, S.; Balamurugan, R.; Sundarrajan, S.; Ramakrishna, S. Nanofibrous structured biomimetic strategies for skin tissue regeneration. *Wound Repair Regen.* **2013**, *21*, 1−16.
(22) Ye, J.; Liao, X.; Xiao, W.; Li, S.; Yang, Q.; Li, G. The effects of molecular weight and supercritical CO2 on the phase morphology of organic solvent free porous scaffolds. *J. Supercrit. Fluids* **2018**, *140*, 279−289.
(23) Li, Z.-H.; Wang, L.; Dai, H.-L.; Wang, X.-Y.; Li, J.-S.; Zhao, Z. Fabrication, characterization, and in vitro evaluation of biomimetic silk fibroin porous scaffolds via supercritical CO2 technology. *J. Supercrit. Fluids* **2019**, *150*, 86−93.
(24) Huang, W.; Ling, S.; Li, C.; Omenetto, F. G.; Kaplan, D. L. Silkworm silk-based materials and devices generated using bio-nanotechnology. *Chem. Soc. Rev.* **2018**, *47*, 6486−6504.
(25) Li, C.; Vepari, C.; Jin, H.-J.; Kim, H. J.; Kaplan, D. L. Electrospun silk-BMP-2 scaffolds for bone tissue engineering. *Biomaterials* **2006**, *27*, 3115−3124.
(26) Hsiao, Y.-C.; Jheng, P.-R.; Nguyen, H. T.; Chen, Y.-H.; Manga, Y. B.; Lu, L.-S.; Rethi, L.; Chen, C.-H.; Huang, T.-W.; Lin, J.-D.; Chang, T.-K.; Ho, Y.-C.; Chuang, E.-Y. Photothermal-Irradiated Polyethyleneimine-Polypyrrole Nanopigment Film-Coated Polyethylene Fabrics for Infrared-Inspired with Pathogenic Evaluation. *ACS Appl. Mater. Interfaces* **2021**, *13*, 2483−2495.
(27) Suo, X.; Zhang, J.; Zhang, Y.; Liang, X.-J.; Zhang, J.; Liu, D. A nano-based thermotherapy for cancer stem cell-targeted therapy. *J. Mater. Chem. B* **2020**, *8*, 3985−4001.
(28) Chen, B.-Q.; Kankala, R. K.; Zhang, Y.; Xiang, S.-T.; Tang, H.-X.; Wang, Q.; Yang, D.-Y.; Wang, S.-B.; Zhang, Y. S.; Liu, G.; Chen, A.-Z. Gambogic acid augments black phosphorus quantum dots (BPQDs)-based synergistic chemo-photothermal therapy through downregulating heat shock protein expression. *Chem. Eng. J.* **2020**, *390*, 124312.
(29) Geng, S.; Zhao, H.; Zhan, G.; Zhao, Y.; Yang, X. Injectable in Situ Forming Hydrogels of Thermosensitive Polypyrrole Nanoplatforms for Precisely Synergistic Photothermo-Chemotherapy. *ACS Appl. Mater. Interfaces* **2020**, *12*, 7995−8005.
(30) Huang, X.; Wu, J.; He, M.; Hou, X.; Wang, Y.; Cai, X.; Xin, H.; Gao, F.; Chen, Y. Combined Cancer Chemo-Photodynamic and Photothermal Therapy Based on ICG/PDA/TPZ-Loaded Nanoparticles. *Mol. Pharmaceutics* **2019**, *16*, 2172−2183.
(31) Wang, Y.; Huang, Q.; He, X.; Chen, H.; Zou, Y.; Li, Y.; Lin, K.; Cai, X.; Xiao, J.; Zhang, Q.; Cheng, Y. Multifunctional melanin-like nanoparticles for bone-targeted chemo-photothermal therapy of malignant bone tumors and osteolysis. *Biomaterials* **2018**, *183*, 10−19.
(32) Xue, Y.; Niu, W.; Wang, M.; Chen, M.; Guo, Y.; Lei, B. Engineering a Biodegradable Multifunctional Antibacterial Bioactive

https://doi.org/10.1021/acsomega.1c02903
ACS Omega 2021, 6, 22213−22223

Nanosystem for Enhancing Tumor Photothermo-Chemotherapy and Bone Regeneration. *ACS Nano* **2020**, *14*, 442−453.
(33) Chen, Q.; Shan, X.; Shi, S.; Jiang, C.; Li, T.; Wei, S.; Zhang, X.; Sun, G.; Liu, J. Tumor microenvironment-responsive polydopamine-based core/shell nanoplatform for synergetic theranostics. *J. Mater. Chem. B* **2020**, *8*, 4056−4066.
(34) Massoumi, B.; Abbasian, M.; Jahanban-Esfahlan, R.; Mohammad-Rezaei, R.; Khalilzadeh, B.; Samadian, H.; Rezaei, A.; Derakhshankhah, H.; Jaymand, M. A novel bio-inspired conductive, biocompatible, and adhesive terpolymer based on polyaniline, polydopamine, and polylactide as scaffolding biomaterial for tissue engineering application. *Int. J. Biol. Macromol.* **2020**, *147*, 1174−1184.
(35) Liu, H.; Mukherjee, S.; Liu, Y.; Ramakrishna, S. Recent studies on electrospinning preparation of patterned, core-shell, and aligned scaffolds. *J. Appl. Polym. Sci.* **2018**, *135*, 46570.
(36) Lu, Q.; Hu, X.; Wang, X.; Kluge, J. A.; Lu, S.; Cebe, P.; Kaplan, D. L. Water-insoluble silk films with silk I structure. *Acta Biomater.* **2010**, *6*, 1380−1387.
(37) Zhang, Y.-Q.; Shen, W.-D.; Xiang, R.-L.; Zhuge, L.-J.; Gao, W.-J.; Wang, W.-B. Formation of silk fibroin nanoparticles in water-miscible organic solvent and their characterization. *J. Nanopart. Res.* **2006**, *9*, 885−900.
(38) Niu, B.; Guo, J.; Guo, X.; Sun, X.; Rao, C.; Liu, C.; Zhang, J.; Zhang, C.; Fan, Y.-Y.; Li, W. (NaPO3)6-assisted formation of dispersive casein-amorphous calcium phosphate nanoparticles: An excellent platform for curcumin delivery. *J. Drug Delivery Sci. Technol.* **2020**, *55*, 101412.
(39) Vautard, F.; Fioux, P.; Vidal, L.; Siffer, F.; Roucoules, V.; Schultz, J.; Nardin, M.; Defoort, B. Use of plasma polymerization to improve adhesion strength in carbon fiber composites cured by electron beam. *ACS Appl. Mater. Interfaces* **2014**, *6*, 1662−1674.
(40) Jahan, M.; Inakpenu, R. O.; Li, K.; Zhao, G. Enhancing the Mechanical Strength for a Microwave Absorption Composite Based on Graphene Nanoplatelet/Epoxy with Carbon Fibers. *Open J. Compos. Mater.* **2019**, *09*, 230−248.
(41) Fu, S.; Hu, H.; Chen, J.; Zhu, Y.; Zhao, S. Silicone resin derived larnite/C scaffolds via 3D printing for potential tumor therapy and bone regeneration. *Chem. Eng. J.* **2020**, *382*, 122928.
(42) Xiang, H.; Yang, Q.; Gao, Y.; Zhu, D.; Pan, S.; Xu, T.; Chen, Y. Cocrystal Strategy toward Multifunctional 3D-Printing Scaffolds Enables NIR-Activated Photonic Osteosarcoma Hyperthermia and Enhanced Bone Defect Regeneration. *Adv. Funct. Mater.* **2020**, *30*, 1909938.
(43) Ma, S.; Moser, D.; Han, F.; Leonhard, M.; Schneider-Stickler, B.; Tan, Y. Preparation and antibiofilm studies of curcumin loaded chitosan nanoparticles against polymicrobial biofilms of Candida albicans and Staphylococcus aureus. *Carbohydr. Polym.* **2020**, *241*, 116254.
(44) Herold, H. M.; Döbl, A.; Wohlrab, S.; Humenik, M.; Scheibel, T. Designed Spider Silk-Based Drug Carrier for Redox- or pH-Triggered Drug Release. *Biomacromolecules* **2020**, *21*, 4904−4912.
(45) Wu, H.; Liu, S.; Xiao, L.; Dong, X.; Lu, Q.; Kaplan, D. L. Injectable and pH-Responsive Silk Nanofiber Hydrogels for Sustained Anticancer Drug Delivery. *ACS Appl. Mater. Interfaces* **2016**, *8*, 17118−17126.
(46) Zhang, N.; Li, M.; Sun, X.; Jia, H.; Liu, W. NIR-responsive cancer cytomembrane-cloaked carrier-free nanosystems for highly efficient and self-targeted tumor drug delivery. *Biomaterials* **2018**, *159*, 25−36.
(47) Zhao, Z.; Chen, C.; Wu, W.; Wang, F.; Du, L.; Zhang, X.; Xiong, Y.; He, X.; Cai, Y.; Kwok, R. T. K.; Lam, J. W. Y.; Gao, X.; Sun, P.; Phillips, D. L.; Ding, D.; Tang, B. Z. Highly efficient photothermal nanoagent achieved by harvesting energy via excited-state intramolecular motion within nanoparticles. *Nat. Commun.* **2019**, *10*, 768.

https://doi.org/10.1021/acsomega.1c02903
ACS Omega 2021, 6, 22213−22223